Monatshefte für Chemie 136, 127–135 (2005)
DOI 10.1007/s00706-004-0229-z

Monatshefte für Chemie
Chemical Monthly
Printed in Austria

$Zr_5Ir_2In_4$ – A Superstructure of the $Lu_5Ni_2In_4$ Type

Mar'yana Lukachuk, Rolf-Dieter Hoffmann, and **Rainer Pöttgen***

Institut für Anorganische und Analytische Chemie and NRW Graduate School of Chemistry, Westfälische Wilhelms-Universität Münster, 48149 Münster, Germany

Received May 6, 2004; accepted (revised) May 26, 2004
Published online October 12, 2004

Summary. $Zr_5Ir_2In_4$ was synthesized by reaction of the elements in a glassy carbon crucible in a water-cooled sample chamber of an induction furnace. The sample was characterized by X-ray diffraction on both powder and single crystals. $Zr_5Ir_2In_4$ crystallizes with a pronounced $Lu_5Ni_2In_4$ type subcell, space group *Pbam*, $a = 1739.5(6)$, $b = 766.3(2)$, $c = 338.9(2)$ pm. Weak additional reflections force a doubling of the subcell c axis. The superstructure of $Zr_5Ir_2In_4$ is of a new type: *Pnma*, $a = 1739.5(6)$, $b = 677.8(2)$, $c = 766.3(2)$ pm, $wR2 = 0.0529$, 1592 F^2 values, and 60 variable parameters. The group-subgroup scheme for the *klassengleiche* symmetry reduction is presented. The formation of the superstructure is most likely due to a puckering effect (size of the iridium atoms). The crystal chemistry of $Zr_5Ir_2In_4$ is briefly discussed.

Keywords. Zirconium compound; Indides; Crystal chemistry; Superstructure.

Introduction

The ternary indides (Ti, Zr, Hf)–*T*–In (*T* = late transition metal) exhibit a peculiar crystal chemistry [1–16]. Although titanium (145 pm), zirconium (160 pm), and hafnium (156 pm) have metallic radii smaller than that of the smallest rare earth element lutetium (173 pm) [17], in some cases these early transition elements form ternary indides that are isotypic with the rare earth metal ones. This is especially the case for the family of RE_2T_2In indides and RE_2T_2Sn stannides [18]. In other cases they form individual structure types [2, 4, 6, 12, 14].

We recently reported on the synthesis and structures of $Zr_5Rh_2In_4$ and $Hf_5Rh_2In_4$ [16]. These indides are isotypic with $Lu_5Ni_2In_4$ [19]. When searching for isotypic iridium compounds we obtained single crystals of $Zr_5Ir_2In_4$, however, this indide crystallizes with a superstructure of the $Lu_5Ni_2In_4$ type. The synthesis and structure determination of this indide are reported herein.

* Corresponding author. E-mail: pottgen@uni-muenster.de

Results and Discussion

$Zr_5Ir_2In_4$ crystallizes with a new superstructure variant of the $Lu_5Ni_2In_4$ type [19]. The rhodium indides $Zr_5Rh_2In_4$ and $Hf_5Rh_2In_4$ crystallize with the subcell structure. Since the crystal chemistry of the latter indides has been discussed in detail in Ref. [16], we only focus on the structural peculiarities of the superstructure here.

As is evident from Table 1, the subcell structure has three zirconium, one iridium, and two indium sites. From a crystal chemical point of view we can distinguish two kinds of zirconium atoms. Zr2 and Zr3 build slightly distorted trigonal prisms around the iridium atoms, and the Zr1 atoms are located in distorted cubes formed by the In1 and In2 atoms. The trigonal prisms $IrZr_6$ are condensed *via* common edges in the *y* direction, and *via* common triangular faces in the *z* direction of the subcell. In the structures of $Zr_5Rh_2In_4$ and $Hf_5Rh_2In_4$ all atoms lie on mirror planes at $z = 0$ and $z = 1/2$.

The only difference between $Zr_5Rh_2In_4$ and $Zr_5Ir_2In_4$ is the small difference in size of the late transition metal atoms, *i.e.* the metallic and covalent radii are 134 and 125 pm for Rh and 136 and 126 pm for Ir [17]. As is evident from Fig. 1, in the superstructure, the zirconium atoms forming the trigonal prisms around the iridium atoms react on the iridium displacement by a displacement in the *xz* plane. A cutout of these trigonal prismatic units is presented in Fig. 2. The displacement of the iridium atoms from the subcell mirror planes is only 9.4 pm. If two iridium atoms move off their prism center towards each other, the zirconium triangle expands,

Table 1. Atomic coordinates and isotropic displacement parameters (pm^2) for $Zr_5Ir_2In_4$; U_{eq} is defined as one third of the trace of the orthogonalized U_{ij} tensor; the subcell iridium position is split and was refined with an isotropic displacement parameter

Atom	*Wyckoff* position	Occupancy %	*x*	*y*	*z*	U_{eq}
subcell (*Pbam*)						
Zr1	2*a*	100	0	0	0	77(2)
Zr2	4*g*	100	0.22134(5)	0.25301(12)	0	119(2)
Zr3	4*g*	100	0.41967(5)	0.13136(11)	0	93(2)
Ir	8*i*	50	0.30626(2)	0.04273(4)	0.46448(19)	74(1)
In1	4*h*	100	0.56731(4)	0.20387(8)	1/2	94(1)
In2	4*h*	96.9(5)	0.85079(4)	0.06795(8)	1/2	94(2)
supercell (*Pnma*)						
Zr1	4*c*	100	0.99906(15)	1/4	0.9992(3)	78(2)
Zr2	4*c*	100	0.22323(12)	1/4	0.7575(2)	95(3)
Zr3	4*c*	100	0.21951(12)	3/4	0.7367(2)	96(3)
Zr4	4*c*	100	0.41661(12)	1/4	0.8728(2)	84(3)
Zr5	4*c*	100	0.42260(12)	3/4	0.8647(2)	81(3)
Ir	8*d*	100	0.30625(2)	0.51392(6)	0.95733(4)	97(1)
In1	8*d*	100	0.56730(4)	0.49447(14)	0.79615(8)	91(1)
In2	8*d*	96.8(4)	0.85080(4)	0.49808(14)	0.93204(8)	95(2)

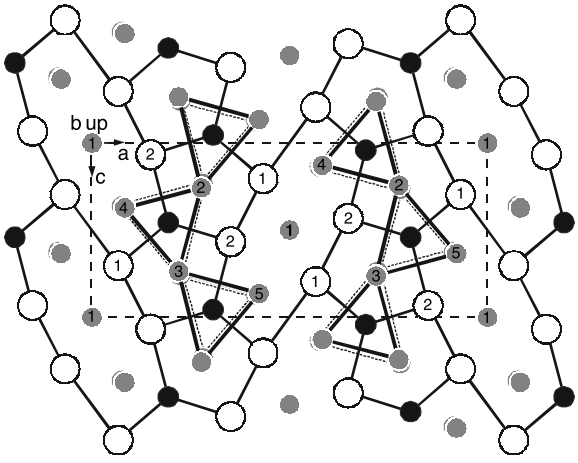

Fig. 1. Projection of the $Zr_5Ir_2In_4$ structure onto the *xz* plane; for clarity, only half of the unit cell in the *y* direction is shown; the zirconium, iridium, and indium atoms are drawn as medium gray, filled, and open circles, respectively; atom designations are indicated; the trigonal prisms around the iridium atoms and the indium network are emphasized

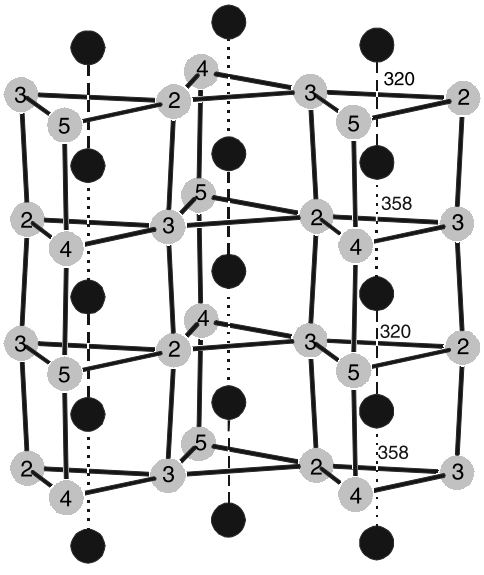

Fig. 2. Cutout of the $Zr_5Ir_2In_4$ structure as depicted in Fig. 1 (view approximately along the *a* direction); some rows of trigonal prismatic units are shown together with some relevant interatomic distances and atom designations

while the triangles above and below contract, leading to a kind of *breathing* of the trigonal prisms. In the neighboring prisms, the Ir and Zr displacements have a phase shift of $y/2$. The displacement of the iridium atoms results in alternating shorter (320 pm) and longer (358 pm) Ir–Ir distances along the *y* direction. The shorter contacts, however, are still much longer than in *fcc* iridium [25] ($d_{\mathrm{Ir-Ir}} = 272$ pm). This clearly indicates that the Ir–Ir interactions in $Zr_5Ir_2In_4$ are most

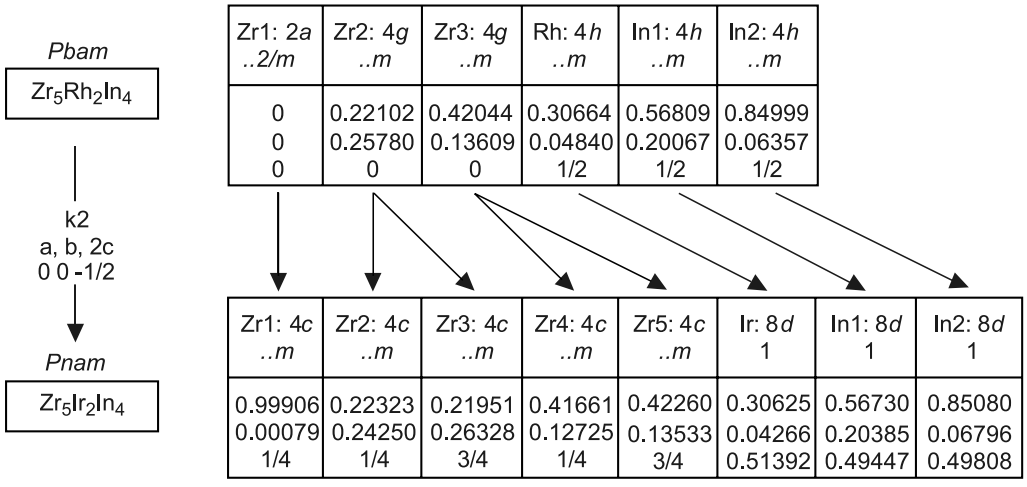

Fig. 3. Group-subgroup scheme in the *Bärnighausen* formalism [26, 27] for the structures of $Zr_5Rh_2In_4$ [16] and $Zr_5Ir_2In_4$; the index for the *klassengleiche* symmetry reduction (k), as well as the unit cell transformation are given; the evolution of the atomic parameters is shown at the right-hand part

likely not bonding and that the formation of the superstructure results from a puckering effect.

The structures of $Zr_5Rh_2In_4$ and $Zr_5Ir_2In_4$ are related by a group-subgroup scheme (Fig. 3). The *Bärnighausen* tree [26, 27] for the *klassengleiche* symmetry reduction of index 2 (k2) from *Pbam* to *Pnam* is shown together with the evolution of the atomic parameters. We have chosen the non-standard setting *Pnam*, for a better comparison of atomic positions. From this scheme we can conclude the following features. The Zr1 atoms that are not involved in the coordination of the iridium atoms almost remain at the ideal subcell positions also in the superstructure. This is also the case for the two indium positions.

The largest displacement occurs for the iridium atoms in the *z* direction (*Pnam* setting). The Zr2 and Zr3 subcell positions split into two zirconium positions each. This allows dislocation of the zirconium atoms in the *xy* plane (*Pnam* setting), leading to the *breathing* of the trigonal prisms.

The mechanism for the formation of the $Zr_5Ir_2In_4$ superstructure is very similar to those for HfRhSn [28], Er_2Au_2Sn [18, 29], U_2Pt_2Sn [30], Zr_3Al_2 [18], $T\text{In}_3$ (T = Co, Ru, Rh, Ir) [31, 32], and $Sc_3Rh_{1.594}In_4$ [33]. All of these structures have late transition metal atoms in trigonal prismatic coordination. A superstructure is formed if the rare earth or actinoid atom is either slightly too small or slightly too large to fit the requirements of the polyanion, thus forcing a distortion. For further details see Ref. [18].

Extended *Hückel* band structure calculations for the averaged subcells and the superstructures of Zr_2Ni_2In and Zr_2Ni_2Sn with similar trigonal prismatic units [8] indicate that the formation of the superstructure is most likely due to packing reasons (size of the zirconium atom). Since the origin of the superstructure formation is very similar for Zr_2Ni_2In and $Zr_5Ir_2In_4$, we assume that such packing reasons also account for $Zr_5Ir_2In_4$ reported herein.

Experimental

Synthesis

Starting materials for the preparation of $Zr_5Ir_2In_4$ were zirconium sponge (Johnson Matthey, >99.5%), rhodium powder (Degussa-Hüls, 200 mesh, >99.9%), and indium tear drops (Johnson Matthey, >99.9%). The elements were weighed in the ideal 5:2:4 atomic ratio and placed in a glassy carbon crucible (SIGRADUR®G, type GAZ006). The latter was put in a water-cooled sample chamber [20] of a high-frequency furnace (Hüttinger Elektronik, Freiburg, Typ TIG 1.5/300). The mixture of the elements was inductively heated under flowing argon until homogenous melting. The argon was purified over silica gel, molecular sieves, and titanium sponge (900 K). The reaction between the elements was visible by a slight heat flash. After the melting procedure the sample was cooled to room temperature within one hour. The light gray sample could easily be separated from the glassy carbon crucible. No obvious reactions of the sample with the crucible could be detected. $Zr_5Ir_2In_4$ is stable in moist air as a compact button as well as a fine-grained powder. Single crystals exhibit metallic luster.

Table 2. Crystal data and structure refinement for $Zr_5Ir_2In_4$

Refined composition	$Zr_5Ir_2In_{3.94(1)}$	
Molar mass	1292.89 g/mol	
Calculated density	9.51 g/cm^3	
Crystal size	$10\times20\times50\ \mu m^3$	
θ range	4° to 32°	
Detector distance	60 mm	
Exposure time	35 min	
ω range; increment	0–180°; 1.0°	
Integr. param. A, B, EMS	13.5; 3.5; 0.010	
Transm. ratio (max/min)	0.577/0.278	
Absorption coefficient	44.6 mm^{-1}	
	subcell	superstructure
Space group	*Pbam*	*Pnma*
Formula units/cell	$Z=2$	$Z=4$
Unit cell dimensions	$a=1739.5(6)$ pm	$a=1739.5(6)$ pm
(powder data)	$b=766.3(2)$ pm	$b=677.8(2)$ pm
	$c=338.9(2)$ pm	$c=766.3(2)$ pm
	V = 0.4518 nm^3	V = 0.9036 nm^3
$F(000)$	1094	2188
Range in *hkl*	±26, ±11, ±5	±26, ±10, ±11
Total no. of reflections	5144	10554
Independent reflections	822 ($R_{int}=0.0440$)	1592 ($R_{int}=0.0722$)
Reflections with $I>2\sigma(I)$	755 ($R_{sigma}=0.0228$)	1208 ($R_{sigma}=0.0364$)
Data/parameters	822/35	1592/60
Goodness-of-fit on F^2	1.247	1.186
Final R indices [$I>2\sigma(I)$]	$R1=0.0295$	$R1=0.0470$
	$wR2=0.0433$	$wR2=0.0493$
R indices (all data)	$R1=0.0354$	$R1=0.0725$
	$wR2=0.0442$	$wR2=0.0529$
Extinction coefficient	0.0012(1)	0.00031(1)
Largest diff. peak and hole	1.69/−1.85 e/Å^3	2.07/−2.19 e/Å^3

Scanning Electron Microscopy

The $Zr_5Ir_2In_4$ crystal investigated on the image plate diffractometer was analyzed by EDX measurements using a Leica 420 I scanning electron microscope with Zr, Ir, and InAs as standards. No impurity elements heavier than sodium were detected. The composition determined by EDX of 49 ± 2 at.-% Zr: 18 ± 2 at.-% Ir: 33 ± 2 at.-% In is close to the calculated ideal composition 45.5 at.-% Zr: 18.2 at.-% Ir: 36.3 at.-% In.

X-Ray Film Data and Structure Refinements

The sample was characterized through its *Guinier* powder pattern using CuKα_1 radiation and α-quartz ($a = 491.30$, $c = 540.46$ pm) as an internal standard. The *Guinier* camera was equipped with an imaging plate system (Fujifilm BAS-1800, 5 min exposure time). The orthorhombic lattice parameters (Table 2) were obtained from a least-squares fit of the *Guinier* data. To ensure correct indexing, the observed pattern was compared to a calculated one [21] using the atomic positions obtained from the structure refinement. The lattice parameters derived from the powders and the single crystals agreed well. The weak superstructure reflections, however, could not be observed on the powder patterns.

Irregularly shaped single crystals of $Zr_5Ir_2In_4$ were isolated from the annealed sample by mechanical fragmentation and subsequently examined by *Laue* photographs on a *Buerger* precession camera (equipped with an imaging plate system Fujifilm BAS-1800) in order to establish suitability for intensity data collection. Intensity data were recorded at room temperature with a *Stoe* IPDS-II image plate diffractometer with graphite monochromatized MoKα (71.073 pm) radiation. The absorption correction was numerical. All relevant crystallographic details for the data collection and evaluation are listed in Table 2.

Table 3. Anisotropic displacement parameters (pm^2) for $Zr_5Ir_2In_4$; U_{eq} is defined as one third of the trace of the orthogonalized U_{ij} tensor; the anisotropic displacement factor exponent takes the form: $-2\pi^2[(ha^*)^2U_{11} + \cdots + 2hka^*b^*U_{12}]$

Atom	U_{11}	U_{22}	U_{33}	U_{23}	U_{13}	U_{12}	U_{eq}
subcell							
Zr1	74(5)	72(4)	84(4)	0	0	−1(4)	77(2)
Zr2	103(4)	192(4)	62(3)	0	0	−21(3)	119(2)
Zr3	112(4)	87(3)	79(3)	0	0	30(3)	93(2)
Ir[a]	74(1)						
In1	84(3)	75(2)	124(3)	0	0	11(2)	94(1)
In2	74(3)	78(3)	130(3)	0	0	−1(2)	94(2)
supercell							
Zr1	73(5)	85(4)	76(4)	0	−2(4)	0	78(2)
Zr2	86(8)	62(5)	136(8)	0	2(6)	0	95(3)
Zr3	99(9)	71(6)	117(7)	0	−19(6)	0	96(3)
Zr4	103(9)	76(6)	73(7)	0	−25(6)	0	84(3)
Zr5	71(9)	86(6)	86(7)	0	−2(6)	0	81(3)
Ir	76(1)	143(2)	73(1)	6(2)	−3(1)	−3(2)	97(1)
In1	86(3)	110(2)	78(2)	−6(3)	−11(2)	5(3)	91(1)
In2	75(3)	128(3)	82(3)	−1(3)	2(2)	−2(3)	95(2)

[a] Only a refinement with an isotropic displacement parameter is reasonable for the split Ir position

The structural relationship of $Zr_5Ir_2In_4$ with $Zr_5Rh_2In_4$ and $Hf_5Rh_2In_4$ [16] was already evident from the *Guinier* powder data, however, the image plate data set of the single crystal readily revealed doubling of the subcell *c* axis. Nevertheless, the structure of the subcell was refined first.

All superstructure reflections were omitted from the data set and the atomic parameters of $Zr_5Rh_2In_4$ [16] were taken as starting values. The subcell structure was refined using Shelxl-97 (full-matrix least-squares on F_o^2) [22] with anisotropic atomic displacement parameters for all sites. This refinement readily revealed an extremely large U_{33} parameter for the iridium site, indicating a displacement from the subcell mirror plane. Therefore, we refined the iridium atoms with split positions *xyz* ($z \approx 0.5$) with 50% occupancy instead of $z = 1/2$. The refined positions and the displacement parameters of the subcell refinement are listed in Table 1. From the Table of the anisotropic displacement parameters (Table 3) it becomes evident, that also the Zr2 positions show unusual displacements, indicating displacements of these atoms in the superstructure as well, but to a lesser extent as compared to the iridium atoms.

The determination of the correct space group was the key to solve the superstructure, but straightforward. The most probable symmetry reductions were an isomorphic step of index 2 (i2) from *Pbam* to *Pbam* or a *klassengleiche* transition of index 2 (k2) from *Pbam* to *Pnam* (non-standard setting of

Table 4. Interatomic distances (pm), calculated with the lattice parameters taken from X-ray powder data of the $Zr_5Ir_2In_4$ superstructure; all distances within the first coordination spheres are listed; standard deviations are all equal or less than 0.3 pm

Zr1:	2	In1	304.6	Zr4:	2	Ir	270.3	In1:	1	Ir	290.0
	2	In1	308.4		2	In1	308.5		1	Zr1	304.6
	1	Zr5	311.5		2	In2	309.7		1	Zr1	308.4
	2	In2	312.1		2	In1	315.6		1	Zr4	308.5
	2	In2	316.4		1	Zr1	319.1		1	Zr5	308.7
	1	Zr4	319.1		2	Zr5	339.1		1	Zr5	310.0
	2	Zr1	338.9		1	Zr5	344.5		1	In2	313.3
Zr2:	2	Ir	276.2		1	Zr2	347.8		1	Zr4	315.6
	2	Ir	284.9		1	Zr3	365.9		1	Zr3	317.4
	2	In2	314.0	Zr5:	2	Ir	267.6		1	Zr2	320.5
	2	In2	319.9		2	In1	308.7		1	In1	331.4
	2	In1	320.5		2	In1	310.0		1	In1	346.4
	2	Zr3	339.3		2	In2	310.6		1	In1	390.5
	1	Zr4	347.8		1	Zr1	311.5	In2:	1	Ir	286.2
	1	Zr3	380.5		2	Zr4	339.1		1	Ir	308.5
	1	Zr5	393.7		1	Zr4	344.6		1	Zr4	309.7
Zr3:	2	Ir	277.4		1	Zr3	366.6		1	Zr5	310.6
	2	Ir	282.6		1	Zr2	393.7		1	Zr1	312.1
	2	In2	313.1	Ir:	1	Zr5	267.6		1	Zr3	313.1
	2	In1	317.4		1	Zr4	270.3		1	In1	313.3
	2	In2	328.1		1	Zr2	276.2		1	Zr2	314.0
	2	Zr2	339.3		1	Zr3	277.4		1	Zr1	316.4
	1	Zr4	365.9		1	Zr3	282.6		1	Zr2	319.9
	1	Zr5	366.6		1	Zr2	284.9		1	Zr3	328.1
	1	Zr2	380.5		1	In2	286.2		1	In2	336.3
					1	In1	290.0		1	In2	341.5
					1	In2	308.5				
					1	Ir	320.0				
					1	Ir	357.8				

Pnma). Careful analyses of the diffractometer data set readily revealed space group *Pnma* to be the correct one. The starting atomic positions were then obtained by an automatic interpretation of direct methods with Shelxs-97 [23] and the superstructure was successfully refined. We used the standard setting *Pnma* for the refinement. For the group-subgroup relation (see Discussion section) the non-standard setting *Pnam* was used for a better comparison with the subcell.

As a check for the correct site assignment and the correct composition, the occupancy parameters were refined in a separate series of least-squares cycles along with the displacement parameters. With the exception of the In2 site, all sites were fully occupied within two standard deviations. In the last cycles, the ideal occupancies were assumed again for these sites. The occupancy parameter of In2 was smaller than 100%. Mixing of indium with iridium on this position can be excluded, since iridium has a larger scattering power. Mixing of indium with zirconium is unlikely because of crystal chemical reasons. We have therefore refined the occupancy parameter of In2 (Table 1) as a least-squares variable in the final cycles. Final difference *Fourier* synthesis revealed no significant residual peaks (see Table 2). The positional parameters and interatomic distances are listed in Tables 1, 3, 4. Further details on the structure refinement may be obtained from Fachinformationszentrum Karlsruhe, D-76344 Eggenstein-Leopoldshafen (Germany), by quoting the Registry No. CSD-414002.

Although the structure refinement converged to low residuals (Table 2), we prefer to calculate separate residuals [24] for the strong subcell and the weak superstructure reflections. Assuming a 4σ cutoff, residuals $R1$ of 0.0285 and 0.1318 were obtained for the 755 subcell and the 453 superstructure reflections, respectively. The weak superstructure reflections accounted for 18% of the total scattering power of the investigated crystal.

Acknowledgements

We thank the Degussa-Hüls AG for a generous gift of iridium powder, Dipl.-Ing. *U. Ch. Rodewald* for the intensity data collection, and *H.-J. Göcke* for the work at the scanning electron microscope. This work was financially supported by the Deutsche Forschungsgemeinschaft. *M. L.* is indebted to the NRW Graduate School of Chemistry for a PhD stipend.

References

[1] Hofer G, Stadelmaier HH (1967) Monath Chem **98**: 408
[2] Kalychak YaM, Zaremba VI, Baranyak VM, Pecharsky VP (1993) Z Kristallogr **205**: 335
[3] Zaremba VI, Gulay LD, Kalychak, Aksel'rud LG (1995) Crystallogr Rep **40**: 334
[4] Zaremba VI, Gulay LD, Kalychak YaM, Bodak OI, Stępień-Damm J (1996) J Alloys Compd **240**: 253
[5] Hulliger F (1996) J Alloys Compd **232**: 160
[6] Gulay LD, Zaremba VI, Kalychak YaM, Stępień-Damm J, Bodak OI (1996) J Alloys Compd **244**: 190
[7] Pöttgen R, Kotzyba G (1996) Z Naturforsch **51b**: 1248
[8] Pöttgen R, Dronskowski R (1997) J Solid State Chem **128**: 289
[9] Gulay LD, Zaremba VI, Kobluck NO (1997) Metally 128
[10] Zumdick MF, Pöttgen R, Müllmann R, Mosel BD, Kotzyba G, Künnen B (1998) Z Anorg Allg Chem **624**: 251
[11] Gulay LD, Zaremba VI, Kalychak YaM, Stępień-Damm J, Kobluck NO (1998) Polish J Chem **72**: 511
[12] Dubenskyy VP, Kalychak YaM, Zaremba VI, Stępień-Damm J (1999) J Alloys Compd **284**: 194
[13] Gulay LD, Zaremba VI, Kalychak YaM, Kobluck NO (1999) Neorg Mater **35**: 572
[14] Zumdick MF, Landrum GA, Dronskowski R, Hoffmann RD, Pöttgen R (2000) J Solid State Chem **150**: 19

[15] Zumdick MF, Pöttgen R, Zaremba VI, Hoffmann RD (2002) J Solid State Chem **166**: 305
[16] Lukachuk M, Pöttgen R (2002) Z Naturforsch **57b**: 1353
[17] Emsley J (1999) The Elements. Oxford University Press, Oxford
[18] Lukachuk M, Pöttgen R (2003) Z Kristallogr **218**: 767
[19] Zaremba VI, Kalychak YaM, Zavalii PYu, Bruskov VA (1991) Krystallografija **36**: 1415
[20] Kußmann D, Hoffmann R-D, Pöttgen R (1998) Z Anorg Allg Chem **624**: 1727
[21] Yvon K, Jeitschko W, Parthé E (1977) J Appl Crystallogr **10**: 73
[22] Sheldrick GM (1997) SHELXL-97, Program for Crystal Structure Refinement. University of Göttingen
[23] Sheldrick GM (1997) SHELXS-97, Program for the Solution of Crystal Structures. University of Göttingen
[24] Hoffmann R-D (1996) RWERT, Program for the Calculation of Residuals for Different Classes of Reflections. University of Münster
[25] Donohue J (1974) The Structures of the Elements. Wiley, New York
[26] Bärnighausen H (1980) Commun Math Chem **9**: 139
[27] Bärnighausen H, Müller U (1996) Symmetriebeziehungen zwischen den Raumgruppen als Hilfsmittel zur straffen Darstellung von Strukturzusammenhängen in der Kristallchemie. University of Karlsruhe and University/GH Kassel
[28] Zumdick MF, Pöttgen R (1999) Z Kristallogr **214**: 90
[29] Pöttgen R (1999) Z Naturforsch **49b**: 1309
[30] Gravereau P, Mirambet F, Chevalier B, Weill F, Fournès L, Laffargue D, Bourée F, Etourneau J (1994) J Mater Chem **4**: 1893
[31] Pöttgen R (1995) J Alloys Compd **226**: 59
[32] Pöttgen R, Hoffmann R-D, Kotzyba G (1998) Z Anorg Allg Chem **624**: 244
[33] Lukachuk M, Zaremba VI, Hoffmann R-D, Pöttgen R (2004) Z Naturforsch **59b**: 182